Structural Biases and Sensitivities of Vegetation Indices

Lynch, P.[1*] and Remmel, T. K.[2]
Faculty of Environmental and Urban Change, York University, Toronto, Canada
E-mail: plynch15@yorku.ca,[1*] remmelt@yorku.ca[2]
**Corresponding Author*

DOI: https://doi.org/10.52939/ijg.v20i11.3679

Abstract
Since the epoch of climate change, observation of forest post-disturbance regeneration by satellite remote sensing has become a major research frontier. However, the monotonic saturation effects of specific reflectance bands may hinder the interpretation of post-disturbance vegetation indexing. We examine how spectral vegetation enhancement index limitations negate widespread implementation. The structural biases and sensitivities of four vegetation indices with potential usefulness for observing post-disturbance forest regeneration are assessed and clarified: the normalized difference vegetation index (NDVI), normalized burn ratio (NBR), near-infrared vegetation index (VI_{NIR}), and the infrared vegetation index (VI_{IR}). Index structures are partitioned in calculation space to model every possible output. Simulated burned, unburned, and global vegetation computational domains for each index are assessed using complex statistical visualizations. Cross-comparison among indices shows that NDVI and NBR exhibit saturation given the upper range of simulated near-infrared (NIR) reflectance inputs (> 0.30) while VI_{NIR} and VI_{IR} display increasing variability given lower inputs in the Green (< 0.10) and Shortwave-infrared (SWIR) (< 0.20), regions of the electromagnetic spectrum. NDVI and NBR display potential for vegetation class separability, while VI_{NIR} and VI_{IR} also display a linear association with forest post-disturbance regeneration stages. VI_{NIR} and VI_{IR} display significant potential for observing forest post-disturbance regeneration compared to traditional vegetation indices.

Keywords: Forestry, Geocomputation, Geographic Information Systems, Remote Sensing, Wildfires

1. Introduction

In the context of global change, the growing attention on the impacts of climate change has exponentially enhanced the interest in plant phenology over the past two decades [1]. Primary research is focused on agriculture, forestry, and classification or mapping, in addition to assessing post-disturbance (e.g., timber harvest and fires) regeneration. According to [2][3] and [4], the collective impacts of both human-caused (e.g., harvests and fires) and natural (e.g., lightning-caused fires and blowdown) disturbances have prompted investigation of forest landscape patterns and regeneration over vast extents. For instance, climate change is becoming more pronounced throughout Canada, producing higher average temperatures, longer and drier summers, and more lightning storms [5]. Referencing [6] and [7], a forest environment altered by climate change, as well as the impact of more frequent and more intense fires, may inherit modified post-disturbance regeneration trajectories. Remote sensing spectral vegetation indices, as reported by [1][8] and [9], are used extensively to assess the instantaneous state and change in the state of vegetation. In [10] and [11], this is seen extensively in forest monitoring and assessment, particularly for tracking post-disturbance regeneration. However, according to [11] [12] and [13], commonly used indices saturate, prohibiting correct interpretation of surface conditions, and are influenced by multiple factors. This study seeks to characterize the impacts of the structural underpinning of the equations used and the input values expected for specific land cover conditions. From [10] and [11], the normalized difference vegetation index (NDVI) is the most widely used spectral enhancement vegetation index for post-disturbance satellite remote sensing.

Vegetation index saturation occurs when a target landscape is covered with vegetation and the specific index is hindered from providing a view of vegetation status or increasing fraction [14]. When viewed from a satellite, index saturation attributed to vegetation's spatial configuration, specifically high leaf-area index and/or high biomass, can affect the detection of plant presence and health assessments by yielding similar or identical values for entirely different vegetation distributions.

Monotonic index saturation primarily attributed to high leaf-area index (LAI) and high biomass and can affect plant presence and health assessments by yielding similar or identical index values for entirely different vegetation conditions, according to [15] and [16]. Complex visual structural models of traditional and advanced indices may be used to identify the influence of saturation effects by simulating the computational domains of spectral vegetation index response across burned and unburned forest land cover [17].

Remote sensing is an effective method for extending field survey findings over a variety of local, regional, or greater extents with the potential to advance current knowledge of environmental processes over the time-series of collected data and beyond with predictive measures; [18][19][20] and [21]. While many survey methods exist to monitor the environment, field methods cannot typically cover such vast extents on a routine basis since remote and hard-to-access sites make field surveys prohibitively expensive. Sensors mounted on orbital satellite platforms record solar radiance reflected from Earth's surface. Reflectance, in the context of this paper, is the percentage, or 0 – 1 ratio, of solar radiance reflected through the atmosphere and received by a remote sensor.

Vegetation indices are intended to characterize greenness, a function of chlorophyll concentration within an instantaneous field of view [22], and may be correlated with things such as plant biophysical properties and canopy structure according to [15] and [23]. Spectral enhancement indices work by mathematically magnifying characteristic spectral properties of target features, often by taking the difference of contrasting spectral responses from key wavelength ranges within the electromagnetic spectrum [24] and normalizing the result to obtain values constrained to a specified range [8]. By enhancing features that characterize vegetation status, spectral vegetation indices assist in classifying target features within a continuous gradient. They assign a single value to each cell in an image, meant to be interpreted as a status indicator of vegetation presence and condition.

Referring to Figure 1, the typical multispectral responses to green vegetation, according to [25] and [26], as well as dry stressed vegetation, according to [27] and [28], in addition to post-disturbance charcoal and severe crown fire burns, according to [29], are shown, superimposed upon the positions of Landsat visible Blue, Green, and Red, Near-infrared (NIR) and Shortwave-infrared (SWIR) bands [30]. Also shown is the typical response for bare soil, according to [31] and [32], since soil can produce "noisy" spectral returns in the absence of vegetation canopies. For instance, [31] and [33] found that the Red/NIR ratio is contingent on the biomass and density of green (chlorophyll-containing) vegetation. The typical signatures for each land cover class indicate significant potential separability in the NIR, SWIR2, and TIR bands. NDVI has been frequently implemented to chronicle vegetation growth cycles with time-series satellite data given its capacity to compensate for sensor angles, lighting conditions, and topographic variations as reported by [9] and [36].

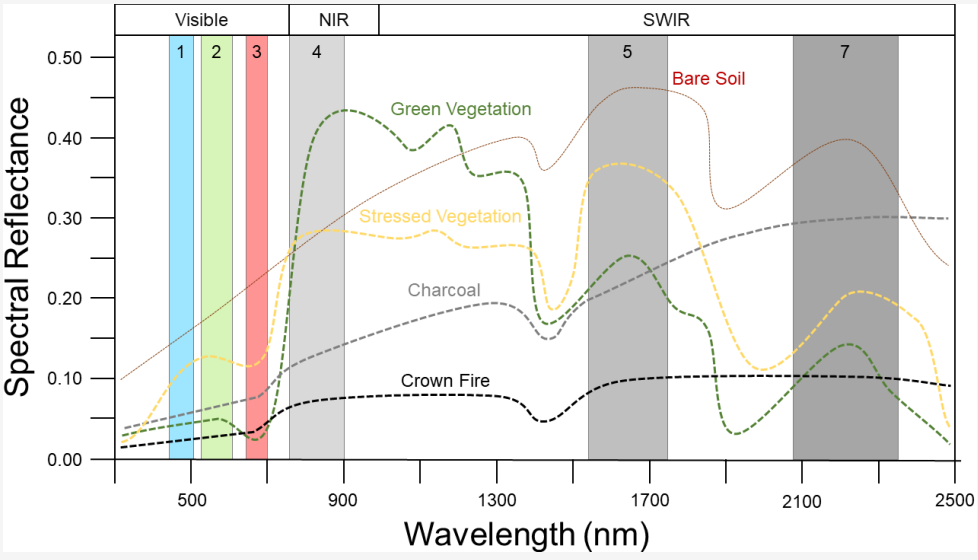

Figure 1: Spectral signatures of typical disturbed and undisturbed land cover types. Modified from [27] [29] [34] and [35]

Chlorophyll absorbs Red and Blue light to drive photosynthesis and therefore green light dominates the reflected visible wavelengths; however, the NIR wavelength is most substantially reflected. NDVI works, as explained by [37] and [38], by calculating the difference between reflectance in the visible Red and invisible NIR and dividing the difference by their sum to normalize the resulting value to a constrained range as presented in equation 1.

$$NDVI = \frac{NIR - Red}{NIR + Red}$$

Equation 1

Vegetation indices incorporating the visible and NIR bands are sensitive to changes in vegetation condition, though they are likewise limited by the presence of shorter vegetation typically covering less area and having less biomass compared to forest trees such as forbs, grasses, and non-woody pioneer flora, which quickly regrow in post-disturbance landscapes rapidly returning the index to pre-disturbance values [11].

NDVI, according to the findings of [12] and [39], is insensitive to variation in vegetation status given NIR reflectance inputs > 0.30, especially with Red inputs < 0.7. For instance, monotonic non-linear saturation typically occurs given LAI > 2 and vegetated fraction (VF) > 60% [12]. LAI is a unitless ratio of two-sided leaf area (m^2) divided by ground area (m^2). VF is the percentage of ground area covered by the vertical projection of leaves, stems, and branches. NDVI typically saturates at NIR > 0.30, meaning the maximum value of the dynamic range levelled off and yielded similar values for different vegetation classes and stages. Here, the dynamic range of an index is defined as the numerical difference between the highest and lowest values for an index calculated for a theoretical remotely sensed satellite scene. The normalized burn ratio (NBR) presented in equation 2 has been used widely to assess post-disturbance regeneration by comparing time-series data; [2] and [10].

$$NBR = \frac{NIR - SWIR2}{NIR + SWIR2}$$

Equation 2

Here, it is crucial to consider the sensitivities of each band incorporated in a vegetation index when selecting the best index for an application. Chlorophyll-rich vegetation exhibits low Red and high NIR reflectance, while burned areas provide low NIR and high SWIR reflectance. SWIR has been found to possess a significant inverse correlation with soil moisture (R^2 > 0.80), according to [40] and [41], the presence of green vegetation, according to [42] and [43], and specific post-fire soil conditions (e.g., ash and charcoal), according to [44] and [45]. NBR has been found to possess a stronger correlation with field survey data of burn severity than NDVI-based methodology [45]. However, NBR has also suffered from saturation during post-disturbance landscape analyses [46]. For instance, comparing field survey data from 289 burn sites in Alaska, USA, it was found that the lowest NBR values did not match the lowest field-assessed severity [47]. According to [15] and [16], significant saturation occurs in the Red and NIR, rendering studies of post-fire regeneration conducted with NDVI and NBR less informative due to reflectance values produced by dense vegetation such as boreal forest stands. Saturation may hinder the transmission of information about post-disturbance regeneration to policymaking as the information will potentially be inaccurate [48].

Previously, numerous indices incorporating both SWIR and thermal-infrared (TIR) (10,400 – 12,500 nm) bands have been tested for observing post-disturbance regeneration [23]. It has been found widely, for instance in [49] [50] and [51], that canopy structure, leaf orientation, leaf water content, and soil moisture content are important factors that determine TIR response. Further, research indicates primary TIR absorption by polysaccharides such as cellulose and leaf surface constituents such as waxes and hairs [52]. Additionally, a strong inverse correlation ($R^2 \geq$ 0.95) has been observed between visible Green (520 – 600 nm) reflectance and Chlorophyll *a* (Chl-*a*) concentrations in global vegetation [53]. A stress-related index incorporating the Green, SWIR, and TIR was proposed by [23], effective for assessing forest regeneration stages, and identifying the time since deforestation. During a study of its usefulness for separating land use and land cover (LULC) types, [54] proposed the name VI_{IR} (infrared vegetation index). VI_{IR} is determined from equation 3.

$$VI_{IR} = \frac{TIR \times Green}{SWIR2}$$

Equation 3

The premise of this index is that where dry (or burned) vegetation will return higher SWIR reflectance, healthier vegetation will return a smaller SWIR denominator yielding higher index values. R^2 = 0.26 (95% confidence) with NDVI compared to 0.93 (99% confidence) with VI_{IR} [23]. In addition to VI_{IR}, [23] proposed the Green, Red, and NIR bands may be effective for regeneration assessments; useful for older sensors onboard satellites that do not feature SWIR or TIR, such as Landsat 1-5 MSS.

We propose the name VI_{NIR} (near-infrared vegetation index); as defined in equation 4 which may be useful for assessing vegetation amount [55].

$$VI_{NIR} = \frac{NIR \times Red}{GREEN}$$

Equation 4

Comparing the index association with post-deforestation regeneration stages, R^2 = 0.50 (95% confidence) [23]. The general premise of this index is that where green reflectance has an inverse relationship with chlorophyll content, healthy vegetation will return a smaller green denominator, yielding a higher index value. As a note of caution, both VI_{NIR} and VI_{IR} may flood to extremely high values due to lower reflectance values resulting from the presence of shadows [56]. Moreover, VI_{NIR} can saturate sharply to extremely high values due to bare soil features that typically possess both Red and NIR reflectance higher than green reflectance values. VI_{NIR} and VI_{IR} possess higher correlations with forest regeneration stages and are expected to provide a more sensitive view of the variability of post-disturbance conditions compared to the traditional NDVI and NBR indices. The intent was to clarify the potential usefulness of NDVI, NBR, VI_{NIR}, and VI_{IR} for assessing the stages of forest post-disturbance regeneration by assessing their structural biases and sensitivities with mathematical models and producing an easily reproducible methodology for predicting index response. Structural biases define the expected outputs given any set of inputs. Input band sensitivities define how much variability an index will possess. Does the structure of an equation for a given index bias the output value, for given inputs? How do index limitations negate widespread implementation?

Vegetation index structures were partitioned into an array-like calculation space to model every possible output within values ranging within established minimum and maximum multispectral and thermal band limits of burned and unburned forest land cover class domains. An inclusive global domain, defined by the upper and lower band input limits of both burned and unburned vegetation allows the simulation of index association with stages of forest regeneration, from burned to unburned. To evaluate how an index equation structure and the bands incorporated may limit the type of information that can be gathered from remotely sensed data, complex statistical visualizations characterize input variables with output metric surfaces.

2. Methods

By defining a mathematical domain with theoretical minimum and maximum response limits for the input bands, each index can be simulated as a continuous number line. Theoretically, this type of study could be conducted without measuring satellite image pixels, given a set of input values justified by a significant body of background research identifying expected electromagnetic band response for relevant land cover types. The findings are considered universally applicable to a wide variety of environments where remotely sensed spectral properties are expected to behave similarly. Table 1 shows simulated multispectral and thermal band input limits, derived from the typical spectral response signatures seen in Figure 1 and the forest land surface temperature (LST) limits defined in [49] and [50], used to define burned, unburned, and inclusive global index domains.

Table 1: Statistical data of simulated bands

Land cover	Green	Red	NIR	SWIR2	TIR (LST °C)	Red × NIR	TIR × Green
Min							
Burned	0.0300	0.0300	0.0600	0.0900	15	0.0018	0.4500
Unburned	0.0400	0.0300	0.3000	0.1500	15	0.0090	0.6000
Global	0.0300	0.0300	0.0600	0.0900	15	0.0018	0.4500
Max							
Burned	0.0500	0.0700	0.1200	0.3000	38	0.0084	1.9000
Unburned	0.1200	0.1000	0.4000	0.2100	38	0.0400	4.5600
Global	0.1200	0.1000	0.4000	0.3000	38	0.0400	4.5600

Model-fitting was performed by adjusting sampled limits to produce theoretical band response distributions and then simulating each index using the continuous number lines. The value of the multiplied inputs of VI_{NIR} and VI_{IR} were treated as independent limits. To understand NDVI, NBR, VI_{NIR}, and VI_{IR} structural biases and sensitivities, each index was simulated within the theoretical multispectral and thermal response domains of burned and unburned forest land cover using array-like structures, as detailed by [17] and [57]. That is, calculations were performed with each index formula using all possible input combinations within the theoretical spectral domains. Simulated domains are theoretical and may possess a significant number of spectral response combinations that most likely will not occur in the real world. Therefore, they provide a limited view of the statistical range of a distribution and variability while preserving an interpretation of central tendency [58]. For instance, green vegetation should not be modeled with the potential to produce negative NDVI values since green vegetation will always reflect more NIR than Red.

Principal Component Analysis (PCA) of mean index response within each land cover class yields a simultaneous comparison of joint sensitivity. Box plots were created to examine potential index variation across the simulated dynamic ranges of simulated burned and unburned land cover classes as well as both classes inclusively (global). Three-dimensional plots, generated by cross-referencing select input values on the *x* and *y*-axes for comparison with the simulated index value on the *z*-axis, provide a view of every possible global computational output as a continuous surface. Global index cross-sections are depicted as transects of box plots with index values grouped by delta (Δ) or multiplier components that define a value increase, which illustrate local variability.

Δ is commonly defined as the difference or expected difference between two values.

3. Results

3.1 Principal Component Analysis

PCA measures the influence of predictor variables on unit vectors expressed as linear angles. Table 2 shows mean index values for each land cover class as derived from simulated multispectral and thermal input computational domains. Loadings are correlation coefficients of the variables used to calculate the principal components (Table 3). Values towards 1 or -1 indicate the input variable strongly influences the vector. Principal component 1 (PC1) represents the axis with the most variation in the data and principal component 2 (PC2) is the axis with the second most variation in the data. Arrow lengths approximate the variance and arrow points correspond to observed scores on the two components. Small angles indicate a correlation between vectors. $\cos^2$ indicates the quality of variable representation (how much a variable is represented) on the PCA for each index, considering the sum of $\cos^2$ values on the PCA is equal to one [59]. Figure 2 illustrates the strong correlation of all four vectors across PC1 given they are known to possess monotonic associations with vegetation status. NDVI, known to have a significant correlation with vegetation Chl-*a* concentrations, is shown to be closely related to NBR, known to have a significant correlation with post-fire burn severity. VI_{NIR} and VI_{IR}, both known to possess significant correlations with stages of vegetation development, are shown to be closely related stress-related indices. The position of VI_{NIR} and VI_{IR} on PC2 indicates they contribute more variability in the direction of linear association compared to NDVI and NBR which are known to saturate, hence opposing vectors.

Table 2: The mean of simulated bands

Land cover	NDVI	NBR	VI_{NIR}	VI_{IR}
Global	0.50	0.05	0.32	14.56
Burned	0.28	-0.34	0.14	7.95
Unburned	0.64	0.41	0.35	14.11

Table 3: Standardized PCA of simulated bands

Land cover	NDVI	NBR	VI_{NIR}	VI_{IR}
Global	0.1602	0.0319	0.4485	0.6372
Burned	-1.0704	-1.0156	-1.1457	-1.1526
Unburned	0.9103	0.9840	0.6972	0.5153

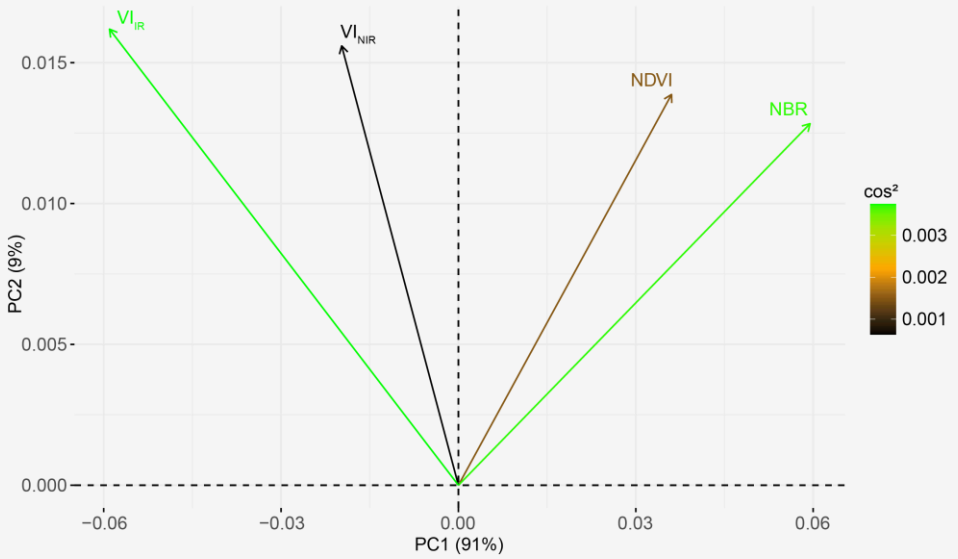

Figure 2: PCA of vegetation indices

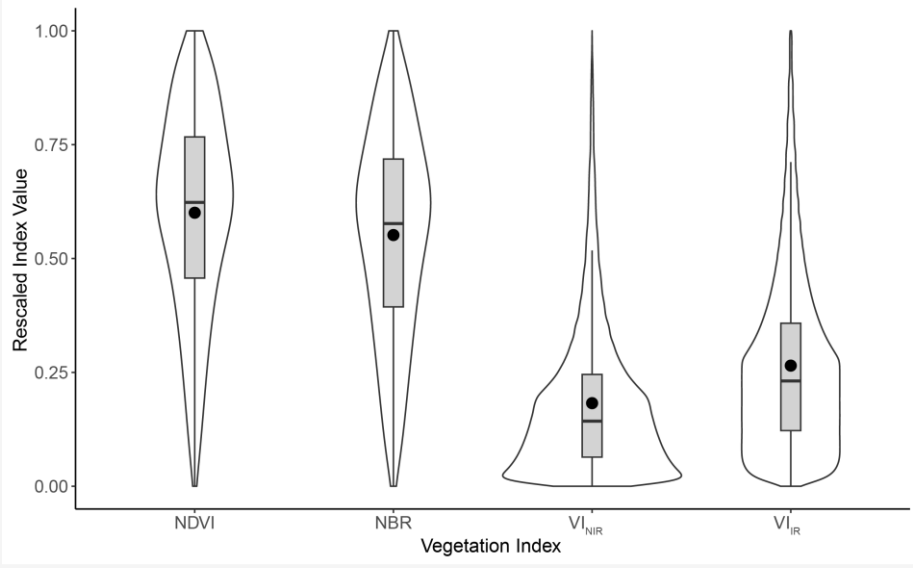

Figure 3: Violin and box plots of vegetation indices

3.2 Vegetation Index Response by Land Cover Class Domain

Simulated global index domains, inclusive of both burned and unburned vegetation, were visualized to identify saturation biases and index similarities and/or differences. Figure 3 shows NDVI, NBR, VI_{NIR}, and VI_{IR} dynamic ranges rescaled to 0.00 – 1.00 to facilitate comparison. Violin plots show the value probability density of all possible values smoothed by a kernel density estimator in addition to the elements of a box plot. The shapes of the violin distributions indicate a bias towards higher NDVI and NBR values compared to VI_{NIR} and VI_{IR}. While the empirical relationships between vegetation indices may result in equally reliable outputs when considering insignificant response differences, functional equivalency is beyond the scope of this paper [60]. Simulated computational domains for NDVI and NBR display distributions that increase in breadth given higher index values and taper off, indicating saturation of higher values. The mathematical structure of VI_{NIR} and VI_{IR} differ from NDVI and NBR. Their simulated domains display distributions grouped towards the lower end of the dynamic ranges. In the comparison of all dynamic class ranges and considering central tendency as an inverse measure of index sensitivity due to saturation to higher values, NDVI and NBR were found to be significantly less sensitive than VI_{NIR} and VI_{IR}.

Notched box plots for all simulated vegetation index burned and unburned land cover value domains yield a view of potential class separability and association with forest status (Figures 4(a)-(d)). Notches are approximated by the interquartile range of a distribution, where non-overlapping notches indicate a significant statistical difference between median values. The notches on Figures 4(b)-(c) are minor, thus barely perceptible, since the simulated domains of VI_{NIR} and VI_{IR} do not possess multiple values at each output level resulting in relatively small confidence limits around the median. In all cases, lower index values are associated with burned vegetation. Saturation characteristics can be determined from Figures 4(a)-(b), where the tendency towards higher NDVI and NBR values and the tapered shape of the distributions indicate monotonic, non-linear association with forest stages across the simulated value ranges having fewer possible simulated outputs nearer the median value. The distributions are approximately normal. Conversely, Figures 4(c)-(d) do not display a tendency towards higher index values and their uniform shapes indicate a monotonic linear association. Simulated index returns for unburned forest are more skewed than burned. In both cases, the distribution of lower values is greater than the tail of higher values.

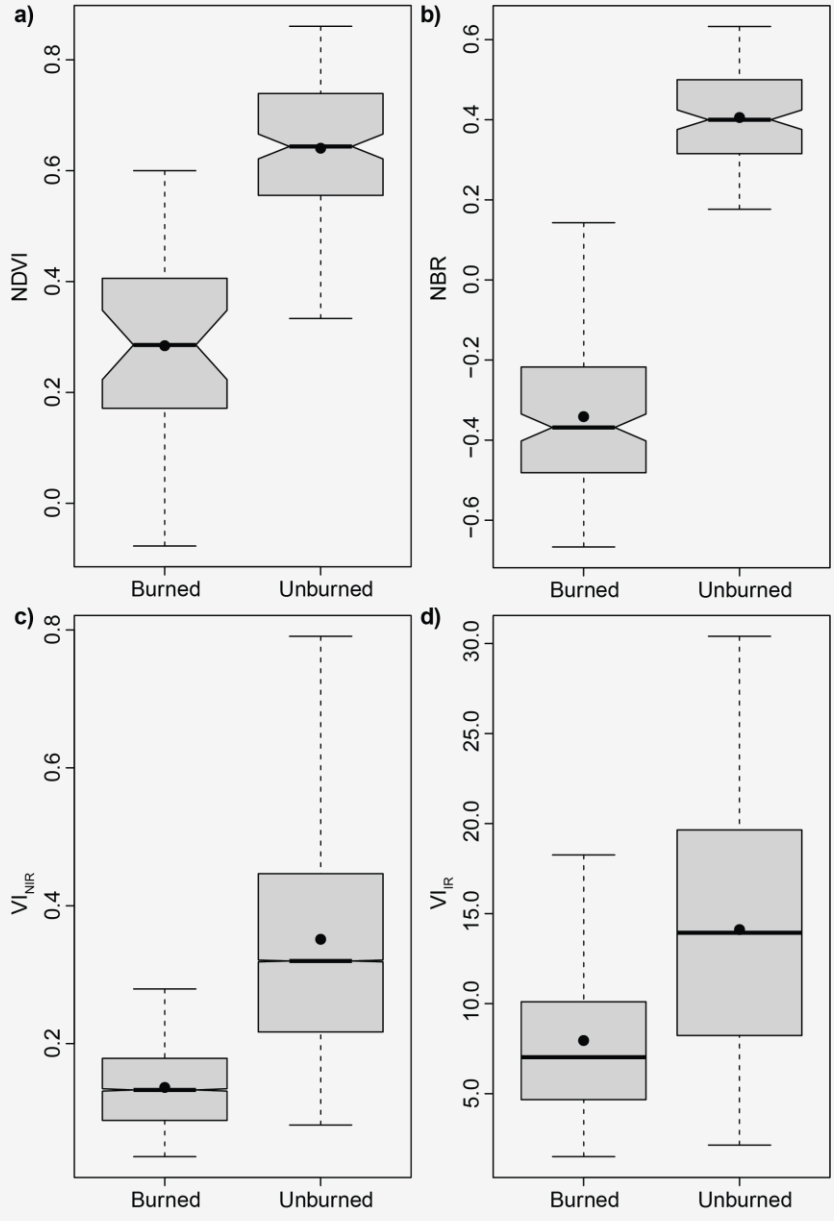

Figure 4: Box plots of burned and unburned for (a) NDVI (b) NBR (c) VI_{NIR} (d) VI_{IR}

Larger dynamic ranges are indicative of greater variability of index response to class-specific features. For instance, the large dynamic range of NBR values for burned vegetation (-0.67 – 0.14) corresponds with the fact that NBR is known to enhance details related to burn severity. NDVI displays different range sizes for burned and unburned vegetation (-0.08 – 0.60 and 0.33 – 0.86) with little class separability, while NBR displays a smaller range for unburned (0.18 – 0.63) and significant separability. In comparison, VI_{NIR} and VI_{IR} display distributions grouped towards the lower end of their dynamic ranges with similar ranges for burned (0.04 – 0.28, 1.50 – 18.26) and unburned (0.08 – 0.79, 2.14 – 30.40) vegetation. Simulated unburned forest returns for VI_{NIR} and VI_{IR} extend farther from the median towards higher values.

3.3 Three-Dimensional Continuous Surfaces and Cross-Sectional Transects

The simulated global domains were summarized by producing three-dimensional plots to visualize index response as a continuous statistical surface (z) to facilitate the interpretation of what combination(s) of input values (x, y) will lead to the possible outputs and the joint-variability among multiple indices (Figures 5(a)–(b)) and Figures 6(a)–(b)). NDVI and NBR display convex structures with increasing index values given larger NIR inputs and decreasing given larger Red or SWIR2 inputs. The output value slope indicates rapid index saturation due to bias associated with NIR > 0.30, in which case the index becomes insensitive to Red < 0.05 and SWIR2 < 0.10. VI_{NIR} and VI_{IR} concave structures increase sharply across multiplied values and decreasing Green or SWIR2 inputs. The slope of the output value indicates gradual saturation towards higher values given smaller denominators.

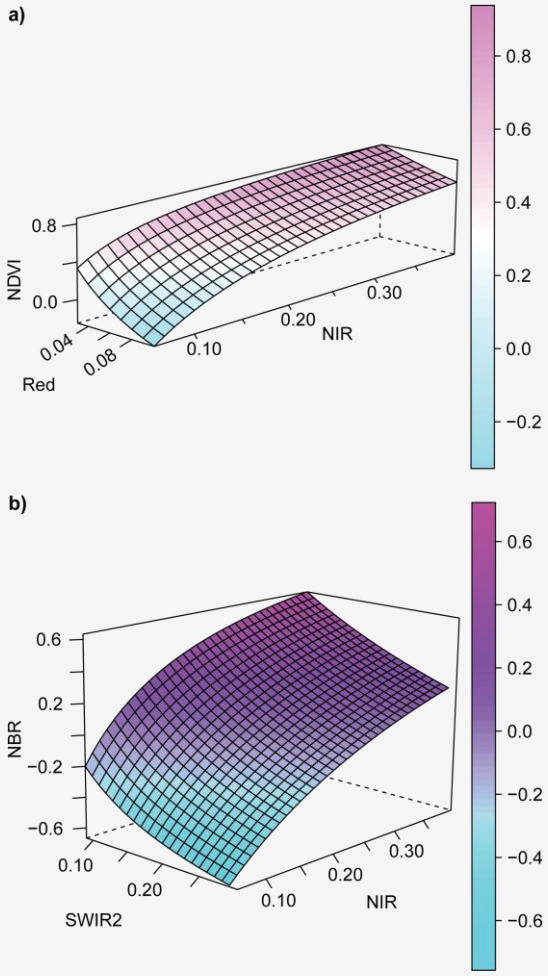

Figure 5: 3D surface of vegetation indices
(a) NIR-RED-NDVI (b) NIR-SWIR2-NBR

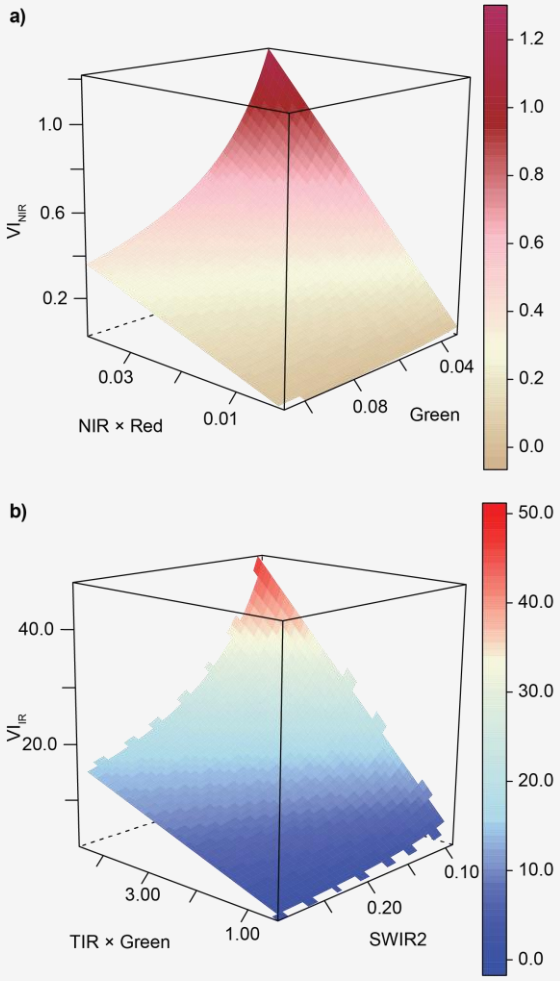

Figure 6: 3D surface of vegetation indices
(a) Green-NIR×Red-VI_{NIR}
(b) SWIR2-TIR×Green -VI_{IR}

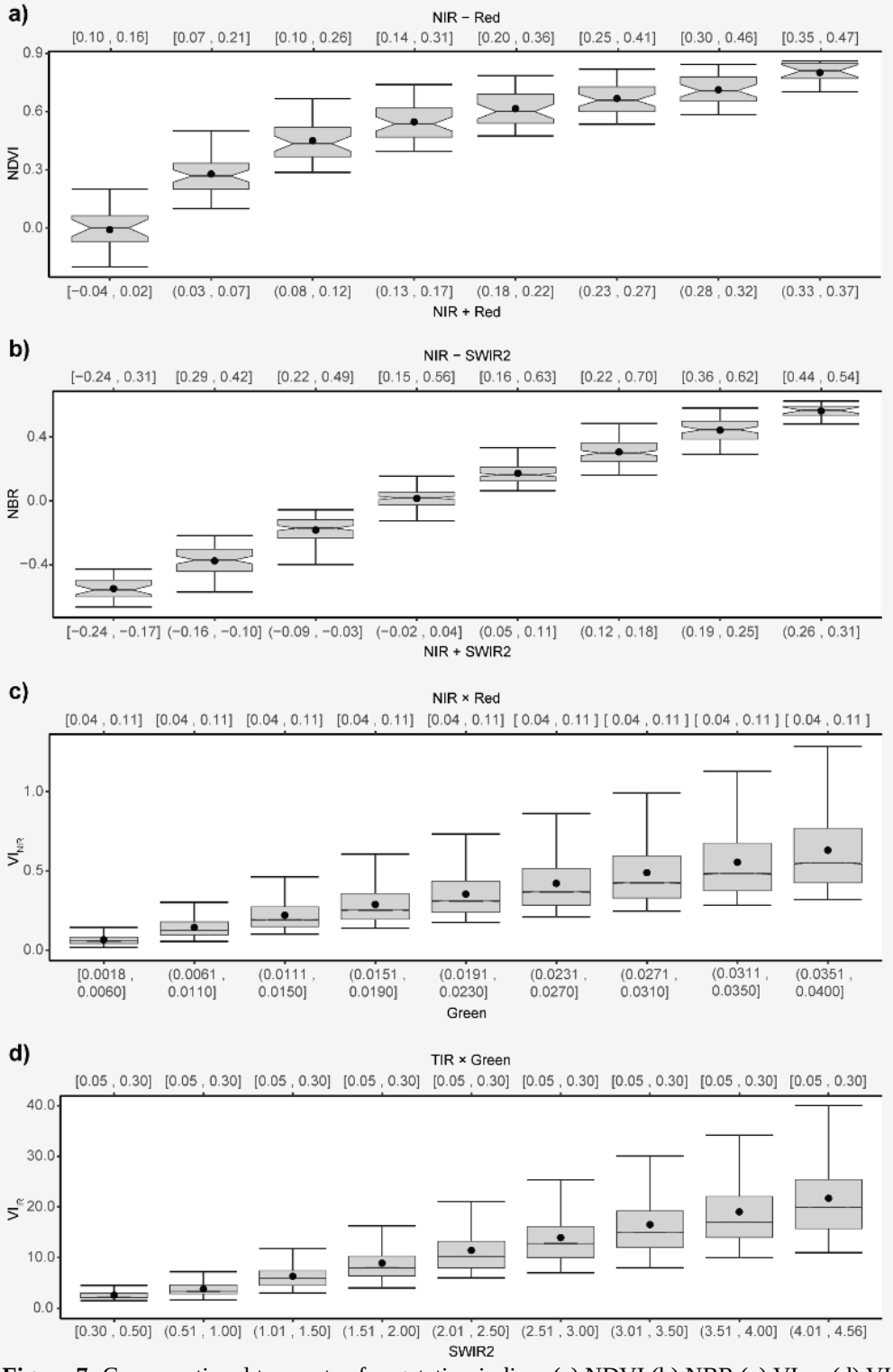

Figure 7: Cross-sectional transects of vegetation indices (a) NDVI (b) NBR (c) VI_{NIR} (d) VI_{IR}

Box plot transects illustrate local variability within index values grouped by band difference, or Δ, (NDVI and NBR) and multiplier (VI_{NIR} and VI_{IR}) components that define an increase in index values (Figures 7(a)–(d)). Index denominators, shown on the upper axis, define association with the target surface. For example, referring to Figure 1, a hypothetical soil target may return a numerator of 0.05 and a denominator of 0.45 (NDVI = 0.11) compared to a hypothetical charcoal target which

may return the same numerator of 0.05 with a denominator of 0.15 (NDVI = 0.33). Here, considering NDVI and NBR, for every range of linearly increasing numerator values, the values of the corresponding range of denominators increase non-linearly, with each maximum value exceeding that of the proceeding range. Moreover, the two NBR denominator groups with the highest values have maximum values lower than that of the previous group, describing lower SWIR2 values compared to previous groups. Conversely, the structure of VI_{NIR} and VI_{IR} dictate the same denominator range for every numerator group. In any case, the index structure provides monotonic separation between unburned and burned vegetation across the dynamic range. NDVI and NBR values depend on the distance between NIR and Red inputs. NDVI and NBR values increase given higher NIR and lower Red inputs, which produce higher Δ values. VI_{NIR} values increase linearly due to the inverse correlation of the Green band denominator with Chl-*a* concentrations as described in Figure 1. Likewise, to VI_{NIR}, VI_{IR} increases linearly due to the inverse correlation of the SWIR2 band with Chl-*a* concentrations, also described in Figure 1.

The NDVI and NBR box plot transects display monotonic non-linear trajectories across their dynamic ranges as the Δ value increases, depicting index saturation. Index transect comparison shows that NDVI and NBR have similar variability across all possible inputs, though NDVI displays the greatest variability between Δ 0.10 – 0.40. VI_{NIR} and VI_{IR} have increasing variability given higher inputs in Red × NIR or SWIR × TIR respectively. The VI_{NIR} and VI_{IR} transects display increasing variability within their dynamic ranges as the multiplied input values increase. While the rate-of-change across NDVI and NBR transects remains relatively constant, the increasing variability across VI_{NIR} and VI_{IR} transects accelerates linearly from one group to the next.

4. Discussion

This study utilized statistical visualizations to assess simulated domains for four vegetation indices with potential usefulness for observing forest post-disturbance regeneration. Cross-comparison among indices within simulations of typical multispectral and thermal band response ranges for burned and unburned vegetation showed that NDVI and NBR are prone to monotonic non-linear saturation of their dynamic ranges, especially NDVI. Conversely, VI_{NIR} and VI_{IR} were found to be much less likely to produce higher index values. PCA measured the variance among indices and showed that NDVI and NBR are closely related compared to VI_{NIR} and VI_{IR}. Both pairs consistently displayed similar variation during each simulation. The lower central tendency of VI_{NIR} may be attributed to the incorporation of dry unburned vegetation in the simulated domains.

Considering index sensitivity to a remotely sensed target, there is a clear association with numerator size on index variance and mean value. The denominator defines feature separation. Removing the denominator during calculation would negate the structural association with the target. For instance, simulations of NBR, VI_{NIR}, and VI_{IR} display significant differences between the dynamic ranges of burned and unburned land cover; NBR displayed a significantly smaller range for unburned in contrast to VI_{NIR} and VI_{IR}. The observed between-class separation identifies all four indices as potentially useful for applications of classification and mapping. Used in tandem, land cover maps can be cross-referenced with VI_{NIR} and VI_{IR} time-series data to observe the health and regeneration trajectories of undisturbed and disturbed forests.

NDVI and NBR surfaces exhibit rapid saturation given NIR > 0.30 as well as Red < 0.05 and SWIR2 < 0.10 values, respectively, according to the expectations of [12] and [39], while VI_{NIR} and VI_{IR} surfaces exhibit more gradual saturation given Green < 0.10 and SWIR2 < 0.20. VI_{NIR} and VI_{IR} flood rapidly given low denominators (possibly attributable to the theoretical presence of shadows or significant moisture content, respectively, as reported in [56] [61] and [62]). Increasing ranges of input NDVI and NBR Δ values across the global domain of forest vegetation, that is, from burned to unburned, produce the expected non-linear saturation effect widely captured in peer-reviewed research, [15] [16] [46] and [47], while increasing input VI_{NIR} and VI_{IR} multipliers produced the linear association expected by [23]. NDVI and NBR display consistent variability across all possible inputs, while VI_{NIR} and VI_{IR} displayed increasing variability given higher multiplier inputs.

5. Conclusion

The intention of this study was to produce an easily replicable methodology for predicting remote sensing spectral enhancement index response, independent of physical study areas, that may be integrated with efforts at any scale. An analysis was made of two traditional spectral vegetation indices (NDVI and NBR) and two advanced spectral vegetation indices (VI_{IR} and VI_{NIR}) by simulating domains based on typical multispectral and thermal response signatures reported in peer-reviewed scientific research. NBR and NDVI displayed little variation across simulated domains since their structural configurations and the bands they

incorporate produce returns with an insensitive upper range of index values when NIR reflectance exceeds 0.30. The results indicate that forest post-disturbance regeneration might be more vividly assessed with VI_{NIR} and VI_{IR} since they express linear association with forest stage, from burned to unburned, and display more local variability when considering higher input values compared to traditional vegetation indices.

The mathematical structure of VI_{NIR} and VI_{IR} possess substantially different computational domains than NDVI and NBR and exhibit greater variability among simulated output ranges, indicating increased sensitivity to vegetation status. It is proposed that VI_{NIR} and VI_{IR} can be useful for observing changes in vegetation status, given their apparent linear associations with the biophysical properties of forest post-disturbance regeneration. NDVI and NBR may not be useful for detailed assessments of post-disturbance landscapes; they may be better suited for applications of classification and mapping requiring significant separation between land cover classes or studies examining only vegetation that yield lower index returns.

Acknowledgments

This work was funded by a Natural Sciences and Engineering Research Council (NSERC) Discovery Grant (RGPIN-2021-03645) to one of the authors.

References

[1] Bajocco, S., Raparelli, E., Teofili, T., Bascietto, M. and Ricotta, C., (2019). Text Mining in Remotely Sensed Phenology Studies: A Review on Research Development, Main Topics, and Emerging Issues. *Remote Sensing*, Vol. 11(23). https://doi.org/10.3390/rs11232751.

[2] Coops, N. C., Hermosilla, T., Wulder, M. A., White, J. C. and Bolton, D. K., (2018). A Thirty Year, Fine-scale, Characterization of Area Burned in Canadian Forests Shows Evidence of Regionally Increasing Trends in the Last Decade. *PLOS ONE*, Vol. 3(5). https://doi.org/10.1371/journal.pone.0197218.

[3] Matasci, G., Hermosilla, T., Wulder, M. A., White, J. C., Coops, N. C., Hobart, G. W., Bolton, D. K., Tompalski, P. and Bater, C.W., (2018). Three Decades of Forest Structural Dynamics Over Canada's Forested Ecosystems using Landsat Time-Series and Lidar Plots. *Remote Sensing of Environment*, Vol. 216, 97-71. https://doi.org/10.1016/j.rse.2018.07.024.

[4] Coops, N. C., Shang, C., Wulder, M. A., White J. C. and Hermosilla, T., (2020). Change in Forest Condition: Characterizing Non-Stand Replacing Disturbances using Time Series Satellite Imagery. *Forest Ecology and Management*, Vol. 474. https://doi.org/10.1016/j.foreco.2020.118370.

[5] Johnston, L. M., Wang, X., Erni, S., Taylor, S. W., McFayden, C. B., Oliver, J. A. and Satockdale, C., (2020). Wildland Fire Risk Research in Canada. *Environmental Reviews*, Vol. 28(2), 164-86. https://doi.org/10.1139/er-2019-0046.

[6] Ice, G. G., Neary, D. G. and Adams, P. W., (2004). Effects of Wildfire on Soils and Watershed Processes. *Journal of Forestry*, Vol. 102, 16-20. https://doi.org/10.1093/jof/102.6.16.

[7] Bond, W. J. and Keane, R. E., (2013). Fires, Ecological Effects of. *In S.A. Levin, Encyclopedia of Biodiversity*, Amsterdam: Elsevier, Academic Press. 435–442.

[8] Xue, J. and Su, B., (2017). Significant Remote Sensing Vegetation Indices: A Review of Developments and Applications. *Journal of Sensors*, Vol. 2017, 1–17. https://doi.org/10.1155/2017/1353691.

[9] Huang, S., Tang, L., Hupy, J. P., Wang, Y. M. and Shao, G., (2020). A Commentary Review on the Use of Normalized Difference Vegetation Index (NDVI) in the Era of Popular Remote Sensing. *Journal of Forestry Research*, Vol. 31, 1-6. https://doi.org/10.1007/s11676-020-01155-1.

[10] Escuin, S., Navarro, R. and Fernández, P., (2008). Fire Severity Assessment by Using NBR (Normalized Burn Ratio) and NDVI (Normalized Difference Vegetation Index) Derived from Landsat TM/ETM Images. *International Journal of Remote Sensing*, Vol. 29(4), 1053–73. https://doi.org/10.1080/01431160701281072.

[11] White, J. C., Wulder, M. A., Hermosilla, T., Coops, N. C. and Hobart, G. W., (2017). A Nationwide Annual Characterization of 25 Years of Forest Disturbance and Recovery for Canada Using Landsat Time Series. *Remote Sensing of Environment*, Vol. 19, 303-321. https://doi.org/10.1016/j.rse.2017.03.035.

[12] Gitelson, A. A., (2004). Wide Dynamic Range Vegetation Index for Remote Quantification of Biophysical Characteristics of Vegetation. *Journal of Plant Physiology*, Vol. 161(2), 165–73. https://doi.org/10.1078/0176-1617-01176.

[13] Ji, L. and Peters, A. J., (2007). Performance Evaluation of Spectral Vegetation Indices Using a Statistical Sensitivity Function. *Remote Sensing of Environment*, Vol. 106(1), 59-65. https://doi.org/10.1016/j.rse.2006.07.010.

[14] Gao, S., Zhong, R., Yan, K., Ma, X., Chen, X., Pu, J., Gao, S., Qi, J., Yin, G. and Myneni, R. B., (2023). Evaluating the saturation Effect of Vegetation Indices in Forests Using 3D Radiative Transfer Simulations and Satellite Observations. *Remote Sensing of Environment*, Vol. 295. https://doi.org/10.1016/j.rse.2023.113665.

[15] Gamon, J. A., Field, C. B., Goulden, M. L., Griffin, K. L., Hartley, A. E., Joel, G., Penuelas, J. and Valenti, H., (1995). Relationships between NDVI, Canopy Structure, and Photosynthesis in Three Californian Vegetation Types. *Ecological Applications*, Vol. 5(1), 28-41 https://doi.org/10.2307/1942049.

[16] Goswami, S., Gamon, J., Vargas, S. and Tweedie, C., (2015). Relationships of NDVI, Biomass, and Leaf Area Index (LAI) for Six Key Plant Species in Barrow, Alaska. *PeerJ PrePrints*. https://doi.org/10.7287/peerj.preprints.913v1.

[17] Remmel, T. K., (2000). *Fire Disturbance Mapping in a Northern Boreal Forest using AVHRR/NDVI Imagery : Comparing Techniques of Change Detection and Substrate Correction.* Master Thesis. Forestry and the Forest Environment FoS., Lakehead University.

[18] NRCan, (2022). *State of Canada's Forests.* Canadian Forest Service.

[19] Canadian Council of Forest Ministers, and Canadian Forest Service, (2007). *Criteria and Indicators of Sustainable Forest Management in Canada: Key Trends and Conditions 2005.* Canadian Forest Service, Ottawa, ON, CA.

[20] Wulder, M. A., White, J. C., Cranny, M., Hall, R. J., Luther, J. E., Beaudoin, A., Goodenough, D. G. and Dechka, J. A., (2008). Monitoring Canada's Forests. Part 1: Completion of the EOSD Land Cover Project. *Canadian Journal of Remote Sensing*, Vol. 34(6), 563-84. https://doi.org/10.5589/m08-066.

[21] Pettorelli, N., Schulte to Bühne, H., Tulloch, A. and Dubois, G., (2018). Satellite Remote Sensing of Ecosystem Functions: Opportunities, Challenges and Way Forward. *Remote Sensing in Ecology and Conservation*, Vol. 4(2), 71-93. https://doi.org/10.10 02/rse2 .59.

[22] Rundquist, B. C., (2002). The Influence Of Canopy Green Vegetation Fraction on Spectral Measurements over Native Tallgrass Prairie. *Remote Sensing of Environment*, Vol. 81(1), 129-135. https://doi.org/10.1016/S0034-4257(01)00339-X.

[23] Boyd, D. S., Foody, G. M., Curran, P. J., Lucas, R. M. and Honzak, M., (1996). An Assessment of Radiance in Landsat TM Middle and Thermal Infrared Wavebands for the Detection of Tropical Forest Regeneration. *International Journal of Remote Sensing*, Vol. 17(2), 249-61. https://doi.org/10.1080/01431169608949003.

[24] Electromagnetic Radiation. *NRCan*. Available: https://www.nrcan.gc.ca/maps-tools-publications/satellite-imagery-air-photos/remote-sensing-tutorials/introduction/electromagnetic-radiation/14621. [Accessed Nov. 4, 2017].

[25] Silván-Cárdenas, J., Corona, N., Galeana-Pizaña, J., Núñez, J. M. and Madrigal, J., (2015). Geospatial Technologies to Support Coniferous Forests Research and Conservation efforts in Mexico. *In Weber, R.P. (Ed.), Old-Growth Forests and Coniferous Forests: Ecology, Habitat and Conservation*, 67–123. Nova Science Publishers, New York, NY, USA.

[26] Goebel, M. and Iwaszczuk, D., (2023). Spectral Analysis of Images of Plants Under Stress Using a Close-Range Camera. *The International Archives of the Photogrammetry, Remote Sensing and Spatial Information Sciences*, Vol. XLVIII-1/W3-2023, 63-69. https://doi. org/10.5194/isprs-archives-XLVIII-1-W3-2023-63-2023.

[27] Papatheodorou, K., (2021). Applied Geology and Geoinformatics for Ground Water Exploration, Protection and Management. *In V. Ashok and C. Maftei (Eds.), Water Safety, Security and Sustainability*, Springer International Publishing, Cham, DE, 23-45.

[28] Rasooli, S. B., Bonyad, A. E. and Pir Bavaghar, M., (2018). Forest Fire Vulnerability Map Using Remote Sensing Data, GIS and AHP Analysis (Case study: Zarivar Lake Surrounding Area). *Caspian Journal of Environmental Sciences*, Vol. 16(4). https://doi.org/10.22124/cjes.2018.3205.

[29] Chuvieco, E., Mouillot, F., van der Werf, G. and San Miguel, J., (2019). Historical Background and Current Developments for Mapping Burned Area from Satellite Earth Observation. *Remote Sensing of Environment*, Vol. 255, 45-64. https://doi.org/10.1016/j.rse.2019.02.013.

[30] Zhang, Y. and Kerle, N., (2008). Satellite Remote Sensing for Near-Real Time Data Collection. *In S. Zlatanova and J. Li (Eds.), Geospatial Information Technology for Emergency Response*, 75–102. Taylor & Francis, London, UK.

[31] Huete, A. R., Jackson, R. D. and Post, D. F., (1985). Spectral Response of a Plant Canopy with Different Soil Backgrounds. *Remote Sensing of Environment*, Vol. 17(1), 37-53. https://doi.org/10.1016/0034-4257(85)90111-7

[32] Storey, E. A., Stow, D. A. and Roberts, D. A., (2020). Evaluating Uncertainty in Landsat-derived Postfire Recovery Metrics Due to Terrain, Soil, and Shrub Type Variations In Southern California. *GIScience & Remote Sensing*, Vol. 57(3), 352-68. https://doi.org/10.1080/15481603.2019.1703287.

[33] Melillos, G., Hadjimitsis, D. G., Issacs, J. C. and Bishop, S. S., (2020). Using Simple Ratio (SR) Vegetation Index to Detect Deep Man-Made Infrastructures in Cyprus. *Detection and Sensing of Mines, Explosive Objects, and Obscured Targets XXV*, Vol. 22. https://doi.org/10.1117/12.2557893.

[34] Introduction to Hyperspectral Imaging. *MicroImages, Inc.* Available: https://www.microimages.com/documentation/Tutorials/hyprspec.pdf. [Accessed Jul. 19, 2024].

[35] Pham, B. D., (2018). *Satellite Remote Sensing of the Variability of the Continental Hydrology Cycle in the Lower Mekong Basin Over the Last Two Decades.* Environmental Sciences FoS., Doctoral Thesis. Sorbonne Université. https://doi.org/10.13140/RG.2.2.27136.07686.

[36] Yengoh, G. T., Dent, D., Lennart, O., Tengberg, A. and Tucker, C., (2016). *Use of the Normalized Difference Vegetation Index (NDVI) to Assess Land Degradation at Multiple Scales: Current Status, Future Trends, and Practical Considerations*, Springer International Publishing, Cham, DE.

[37] Kriegler, F., Malila, W. A., Nalepka, R. F. and Richardson, W., (1969). Preprocessing Transformations and their Effects on Multispectral Recognition. *Proceedings of the Sixth International Symposium on Remote Sensing of Environment*. October 13-16, 1969. Ann Arbor, MI, USA

[38] Rouse, J. W., Haas, R. H., Schell, J. A. and Deering, D. W., (1973). Monitoring Vegetation Systems in the Great Plains with ERTS: SP-351. *Proceedings of 3rd Earth Resources Technology Satellite Symposium*. December 10-14, 1973. Greenbelt, MA, US.

[39] Liu, F., Qin, F. and Zhan, Z., (2012). A Novel Dynamic Stretching Solution to Eliminate Saturation Effect in NDVI and its Application in Drought Monitoring. *Chinese Geographical Science*, Vol. 22(6), 683-94. https://doi.org/10. 1007/s11769-012-0574-5.

[40] Ullah, S., Skidmore, A. K., Ramoelo, A., Groen, T. A., Naeem, M. and Ali, A., (2014). Retrieval of Leaf Water Content Spanning the Visible to Thermal Infrared Spectra. *ISPRS Journal of Photogrammetry and Remote Sensing*, Vol. 93, 56-64. https://doi.org/10.1016/j.isprsjprs.2014.04.005.

[41] Fabre, S., Xavier, B. and Lesaignoux, A., (2015). Estimation of Soil Moisture Content from the Spectral Reflectance of Bare Soils in the 0.4–2.5 µm Domain. *Sensors*, Vol. 15(2), 3262-81. https://doi.org/10.3390/s150203262.

[42] Blackburn, G. A., (1999). Relationships between Spectral Reflectance and Pigment Concentrations in Stacks of Deciduous Broadleaves. *Remote Sensing of Environment*, Vol. 70(2), 224-37. https://doi.org/10.1016/S0034-4257(99)00048-6.

[43] Boyd, D. S. and Petitcolin, F., (2004). Remote Sensing of the Terrestrial Environment Using Middle Infrared Radiation (3.0-5.0 µm). *International Journal of Remote Sensing*, Vol. 25, 3343-68. https://doi.org/10.1080/01431160310001654356.

[44] Boucher, J., Beaudoin, A., Hébert, C., Guindon, L. and Bauce, E., (2017). Assessing the Potential of the Differenced Normalized Burn Ratio (dNBR) for Estimating Burn Severity tn Eastern Canadian Boreal Forests. *International Journal of Wildland Fire*, Vol. 26(1). https://doi.org/10.1071/WF15122.

[45] van Gerrevink, M. J. and Veraverbeke, S., (2021). Evaluating the Near and Mid Infrared Bi-Spectral Space for Assessing Fire Severity and Comparison with the Differenced Normalized Burn Ratio. *Remote Sensing*, Vol. 13(4). https://doi.org/10.3390/rs13040695.

[46] Delcourt, C. J. F., Combee, A., Izbicki, B. and Mack, M. C., (2021). Evaluating the Differenced Normalized Burn Ratio for Assessing Fire Severity Using Sentinel-2 Imagery in Northeast Siberian Larch Forests. *Remote Sensing*, Vol. 13(12). https://doi.org/10.3390/rs13122311.

[47] Allen, J. L. and Sorbel, B., (2008). Assessing the Differenced Normalized Burn Ratio's Ability to Map Burn Severity in the Boreal Forest and Tundra Ecosystems of Alaska's National Parks. *International Journal of Wildland Fire*, Vol. 17(4). https://doi.org/10.1071/WF08034.

[48] De Leeuw, J., Georgiadou, Y., Kerle, N., De Gier, A., Inoue, Y., Ferwerda, J., Smies, M. and Narantuya, D., (2010). The Function of Remote Sensing in Support of Environmental Policy. *Remote Sensing*, Vol. 2(7), 1731–50. https://doi.org/10.3390/rs2071731.

[49] Mildrexler, D. J., Zhao, M. and Running, S. W., (2011). A Global Comparison between Station Air Temperatures and MODIS Land Surface Temperatures Reveals the Cooling Role of Forests. *Journal of Geophysical Research*, Vol. 116(G3). https://doi.org/10.1029/2010JG001486.

[50] Xue, S. Y., Xu, H. Y., Mu, C. C. and Wu, T. H., (2021). Changes in Different Land Cover Areas and NDVI Values in Northern Latitudes from 1982 to 2015. *Advances in Climate Change Research:* Vol. 12(4), 456–65. https://doi.org/10.1016/j.accre.2021.04.003.

[51] Shaik, R. U., Jallu, S. B. and Doctor, K., (2023). Unveiling Temperature Patterns in Tree Canopies Across Diverse Heights and Types. *Remote Sensing*, Vol. 15(8). https://doi.org/10.3390/rs15082080.

[52] Neinavaz, E., Schlerf, M., Darvishzadeh, R., Gerhards, M. and Skidmore, A. K., (2021). Thermal Infrared Remote Sensing of Vegetation: Current Status and Perspectives. *International Journal of Applied Earth Observation and Geoinformation*, Vol. 102. https://doi.org/10.1016/j.jag.2021.10241.

[53] Gitelson, A. A., Kaufman, Y. J. and Merzlyak, M. N., (1996). Use of a Green Channel in Remote Sensing of Global Vegetation from EOS-MODIS. *Remote Sensing of Environment*, Vol. 58(3), 289-98. https://doi.org/10.1016/S0034-4257(96)00072-7.

[54] Van, T. T., (2009). *Relationship of Thermal Properties and Vegetation Indices in Remote Sensing Land Cover Mapping*. 30th Asian Conference on Remote Sensing. October 18-23, Beijing, China. Asian Association on Remote Sensing (AARS).

[55] Curran, P., (1980). Multispectral Remote Sensing of Vegetation Amount. Progress in Physical Geography. *Earth and Environment*, Vol. 4(3), 315–31. https://doi.org/10.1177/030913338000400301.

[56] Zhang, L., Sun, X., Wu, T. and Zhang, H., (2015). An Analysis of Shadow Effects on Spectral Vegetation Indexes Using a Ground-Based Imaging Spectrometer. *IEEE Geoscience and Remote Sensing Letters*, Vol. 12(11), 2188-2192. https://doi.org/10.1109/LGRS.2015.2450218.

[57] Lu, M., Appel, M. and Pebesma, E., (2018). Multidimensional Arrays for Analysing Geoscientific Data. *ISPRS International Journal of Geo-Information*, Vol. 7(8). https://doi.org/10.3390/ijgi7080313.

[58] González-Estrada, E. and Cosmes, W., (2019). Shapiro–Wilk test for Skew Normal Distributions Based on Data Transformations. *Journal of Statistical Computation and Simulation*, Vol. 89(17), 3258-3272. https://doi.org/10.1080/00949655.2019.1658763.

[59] Abdi, H. and Williams, L. J., (2010). Principal Component Analysis. *WIREs Computational Statistics*, Vol. 2(4), 433-459. https://doi.org/10.1002/wics.101.

[60] Perry, C. R. and Lautenschlager, L. F., (1984). Functional Equivalence of Spectral Vegetation Indices. *Remote Sensing of Environment*, Vol. 14, 169–82.

[61] Salama, R. B., (2011). Remote Sensing of Soils and Plants Imagery. *In J. Gliński, J. Horabik, and J. Lipiec (Eds.), Encyclopedia of Agrophysics*, Springer, Netherlands. 681–93. https://doi.org/10.1007/978-90-481-3585-1.

[62] Młynarczyk, A., Konatowska, M., Królewicz, S., Rutkowski, P., Piekarczyk, J. and Kowalewski, W., (2022). Spectral Indices as a Tool to Assess the Moisture Status of Forest Habitats. *Remote Sensing*, Vol. 14(17). https://doi.org/10.3390/rs14174267.